SSRG International Journal of Electrical and Electronics Engineering
ISSN: 2348-8379/ https://doi.org/10.14445/23488379/IJEEE-V10I7P118

Volume 10 Issue 7, 199-210, July 2023

Original Article

A PSO-ANFIS MPPT-Based 3-Phase Series Resonant Converter with DLLC Tanks for Hybrid Solar Wind Battery System with DC-Load

Heena Parveen[1], A. Raghu Ram[2]

[1,2]*Department of EEE, JNTUH College of Engineering, Telangana, India.*

[1]*Corresponding Author : parveenheena21@gmail.com*

Received: 27 April 2023 Revised: 26 June 2023 Accepted: 12 July 2023 Published: 31 July 2023

Abstract *- This paper shows a three-phase series resonant DC-DC boost converter simulation model with double LLC resonant tanks (SRC-W-DLLC-RTs) for a hybrid solar wind system (HSWS) with battery energy storage for a DC load. An intrinsic drawback of hybrid solar-wind technology is its intermittent and weather-dependent output voltage. An MPPT control algorithm-based DC-DC converter, which offers interfaces between a hybrid system and a DC load, can overcome this issue. Solar and wind power systems require separate converters. The lead-acid battery bank with a 3-phase interleaved bidirectional DC-DC buck-boost converter maintains a steady voltage at the DC link. The hybrid system is controlled by an adaptive neuro-fuzzy inference system-based particle swarm optimization (ANFIS-PSO)-MPPT control technique to maximize output. A variable frequency modulation approach generates gating pulses for the converter's switches. An ANFIS-PSO MPPT control algorithm-based resonant converter is simulated with MATLAB using SIMULINK for DC load, and its performance is analyzed for the suggested system for different load conditions.*

Keywords *- Hybrid solar-wind system, Lead acid battery bank, 3-phase interleaved bidirectional DC-DC boost converter, SRC-W-DLLC-RTs, Variable frequency modulation, ANFIS–PSO MPPT control algorithm, R-load (DC-load).*

1. Introduction

Using clean and sustainable energy sources is essential because of the adverse environmental effects of burning petroleum-based materials and the depletion of their stocks. These green energies, which include solar energy (SE), wind energy (WE), and fuel cells, can be employed as generation systems [1, 2].

Renewable energy sources' significant limitations are that they are erratic and that the weather influences the creation of electrical energy. Unreliable power output is produced by non-traditional sources like SE and WE power systems [3, 4].

We should run these power plants together as a single unit for a continuous electricity supply to overcome this issue. The system becomes more effective due to this combined method of operation. Using batteries as a storage component, the combined electricity generation will provide a continuous power source for residential applications [5, 6].

The unreliability of the power outputs and fulfilling the load demand are also significant problems in renewable power generation systems[7]. To get around this, we need advanced power electronics DC-DC converters with high conversion efficiency to keep the voltage on the DC bus steady and meet the load demand [8, 9]. DC-DC converters are classified into soft-switching (or resonant) converters and hard-switching converters (HSC). Compared to HSC, resonant DC-DC converters have a higher conversion rate, smaller magnetic components like transformers and passive filters, the ability to function at high switching frequencies, and an efficient power density [10, 11].

Additionally, RPCs employ various techniques to fulfil soft-switching requirements rather than adding supplementary equipment to each switch. RPCs organize as a Resonant Tank Network (RTN) with the converter connected in cascade to two, three, or more reactive elements [12]. RTN types can also be divided into groups according to how their tank elements are connected to them and how many of them there are [13].

The two most common designs of the two-element RTN type are parallel resonant converters (PRC) and series resonant converters (SRC). The LLC and LCC are three-element RTNs, but the series-parallel resonant converter (SPRC), like the LCLC, is a multi-element RTN [14, 15].

Furthermore, the relation between the resonant frequency (F_r) and the switching frequency (F_s) is required for the power resonant converter's soft-switching approach. When F_s is less than F_r, the converter will perform zero current switching (ZCS) on all switches. When F_s is greater than F_r, zero voltage switching (ZVS) is achievable [16].

This research uses an ANFIS-PSO MPPT algorithm-based SRC with DLLC-RTs for an HSWS with storage capacity as a simulation model [17]. The backup energy stored in the battery is utilized to meet the linked load requirement of this system when SE, and WE are not available. Gating pulses for the converter switches are produced using a variable frequency modulation approach.

For the solar-wind system, the suggested converter's performance is examined, and FFT analysis is performed to examine the amount of THD transmitted to load from the converter.

The remaining parts of the work are divided into sections: Section II details the hybrid system's circuit structure, which involves designing the suggested converter and MPPT method. Part III contains the simulation model. Section IV presents the simulation findings. Finally, in Section V, the study is summarized and concluded.

2. Proposed System Layout

The system shown in Figure 1 comprises solar panels and permanent magnet synchronous generator (PMSG)-based vertical axis wind turbine (VAWT) units connected to a DC link via a DC-to-DC converter. A battery bank is also connected through a three-phase buck-boost interleaved converter. An R-load is taken as a DC-Load [18, 19].

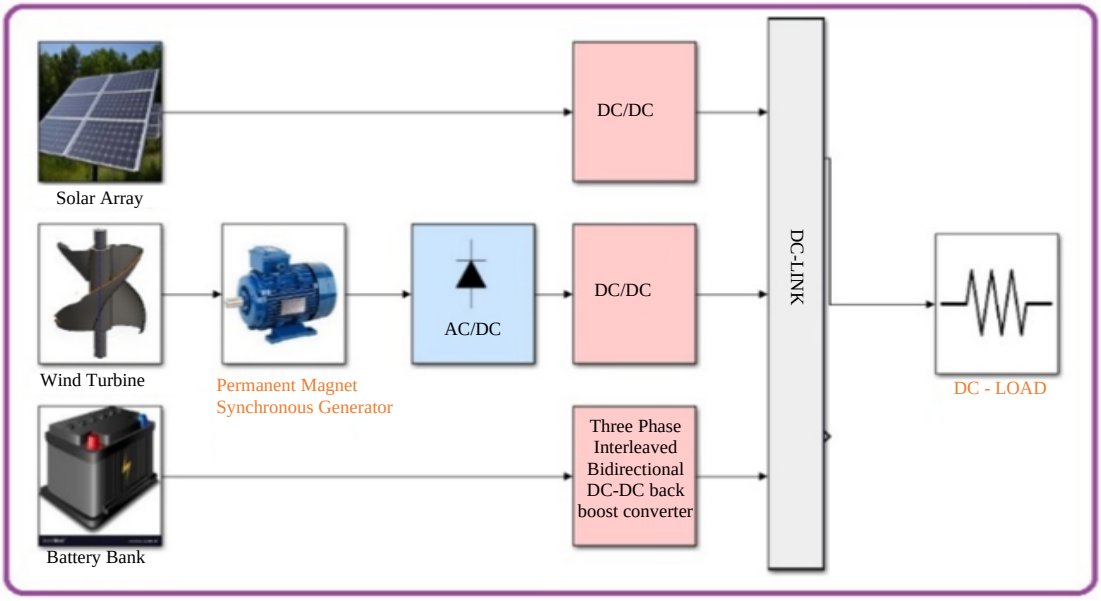

Fig. 1 Proposed hybrid solar-wind system model

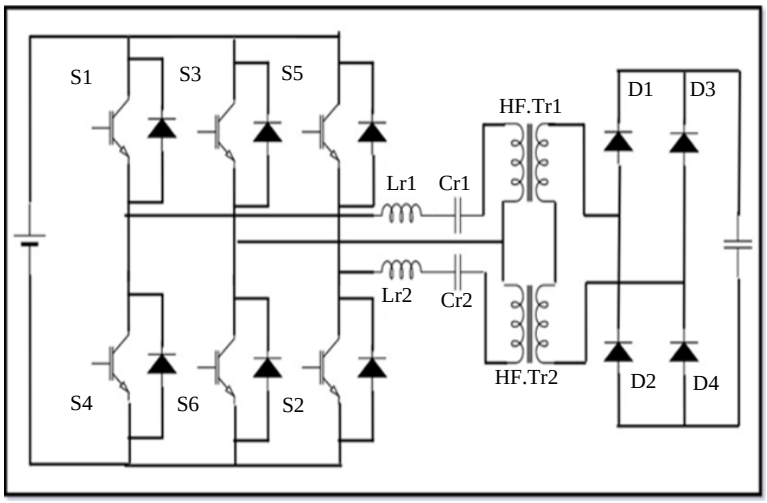

Fig. 2 The proposed converter

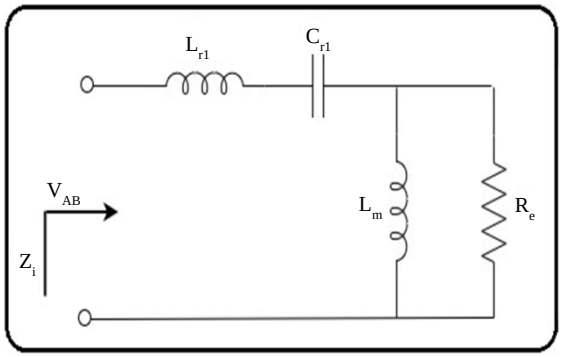

Fig. 3 The AC circuit model for a single LLC RTs

2.1. Design of Proposed Converter

Figure 2 presents the DC/DC converter's circuit design, which consists of a 3-phase inverter with two LLC RTs, with each RT formed by the resonant inductance (L_r), resonant capacitance (C_r), and magnetizing inductance (L_m) of the high frequency (HF) transformer. Both transformers' secondary windings are series-connected and are coupled to the single-phase full-bridge diode rectifier [20].

2.1.1. Design of Resonant Tanks

To provide an equal F_r for the converter for simple design consideration, the RT's variables, such as currents and voltages (IL_{r1}, IL_{r2}, VC_{r1}, and VC_{r2}), are balanced using the same tank parameters.

As the corresponding circuit in Figure 3 shows, one of the LLC RTs receives the voltage V_{AB}. The output voltage gain of RT is increased by dividing the voltage across the I/P and O/P impedances. The transformer winding ratio (n) transfers the effective resistance (R_e) from the secondary side components to the primary and the following formulas may express the converter gain equation:

$$\text{Input Impedance } (Z_i) = X_{Lr} + X_{Cr} + \left(\frac{X_{Lm}R_e}{R_e+X_{Lm}}\right) \quad (1)$$

$$\text{Output impedance } (Z_0) = \frac{X_{Lm}R_e}{R_e+X_{Lm}} \quad (2)$$

$$M=\frac{Z_0}{Z_i} = \frac{\frac{jw_sL_{m.}R_e}{R_e+jw_sX_{Lm}}}{jw_sL_r-\frac{j}{w_sC_r}+\frac{jw_sL_{m.}R_e}{R_e+jw_sX_{Lm}}} \quad (3)$$

Provided that the parameters of the second tank are the same as those of the first, obtaining the output AC voltage gain of the second tank is equivalently attainable. As a result, the parameters of both tanks can be calculated using the given formulas:

$$\text{Resonance Frequency } (f_r) = \frac{1}{2\pi\sqrt{L_rC_r}} \quad (4)$$

$$\text{Inductance Ratio } (A_L) = \frac{L_m}{L_r} \quad (5)$$

$$\text{Characteristic Impedance } (Z_C) = \sqrt{\frac{L_r}{C_r}} = 2\pi f_r L_r = \frac{1}{2\pi f_r C_r} \quad (6)$$

$$\text{Load Quality Factor } (Q) = \frac{Z_O}{R_e} = \frac{w_rL_r}{R_e} = \frac{1}{w_rC_rR_e} \quad (7)$$

$$\text{Effective ac resistance } (R_e) = \frac{8n^2}{\pi^2}R_L \quad (8)$$

Where the angular resonant frequency = W_r. The Values of L_r and C_r can be obtained by:

$$L_r = \frac{QR_e}{w_r} \quad (9)$$

$$C_r = \frac{1}{L_r \times w_r^2} \quad (10)$$

2.1.2. Modes of Operation

Figure 4 depicts the proposed converter's operational modes.

2.2. Hybrid ANFIS–PSO-Based MPPT Controller

For designers today, learning and updating ANFIS requirements is a difficult task. The PSO delivers faster and easier updating convergence velocity than gradient approaches [21, 22]. Moreover, the PSO does not demand the determination of initial parameters or a learning rate. The ANFIS controller's design, which consists of five layers in total, with antecedents and conclusions serving as the main components, is shown in Figure 5.

An ANFIS-PSO MPPT control's intricate flowchart arrangement is shown in Figure 6. Before the error is minimised to the minimum possible degree, an improved hybrid MPPT technique captures fuzzy data with learnt learning rules for correct membership value modification.

The learnt system transforms into a hybrid MPPT controller as membership parameters are altered. The centroid technique is used to modify the converter duty ratio during defuzzification [23].

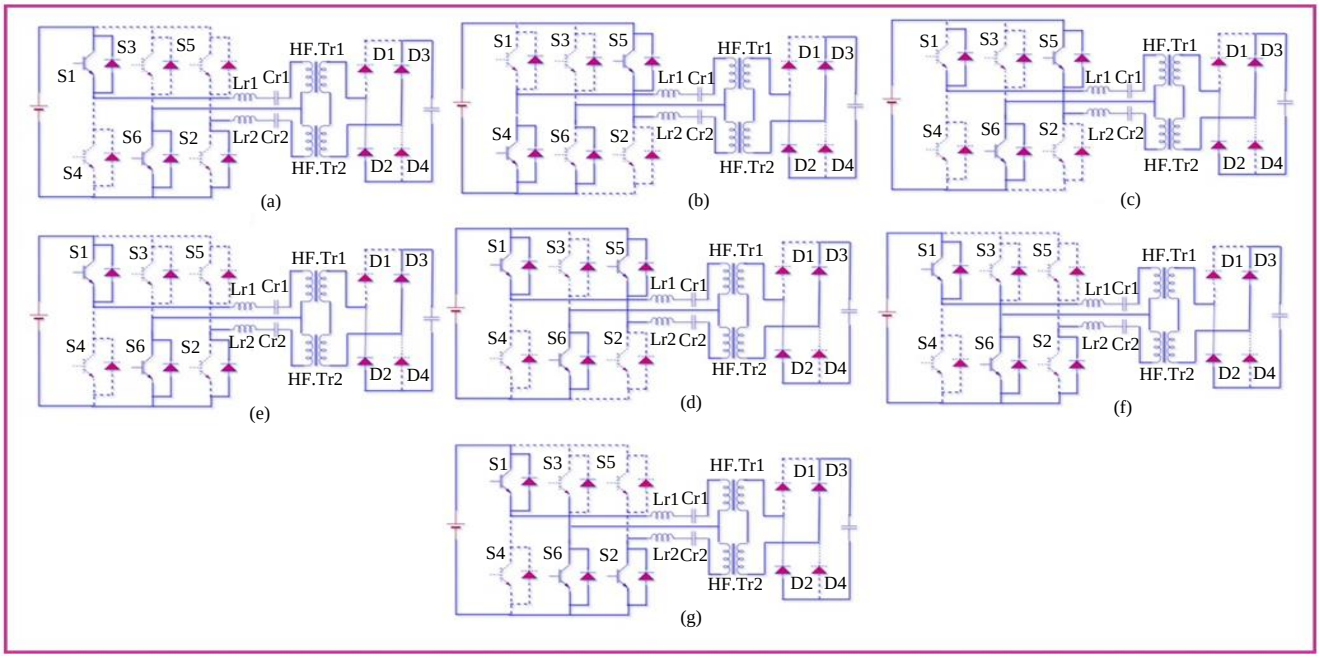

Fig. 4 Operating modes of proposed resonant converter

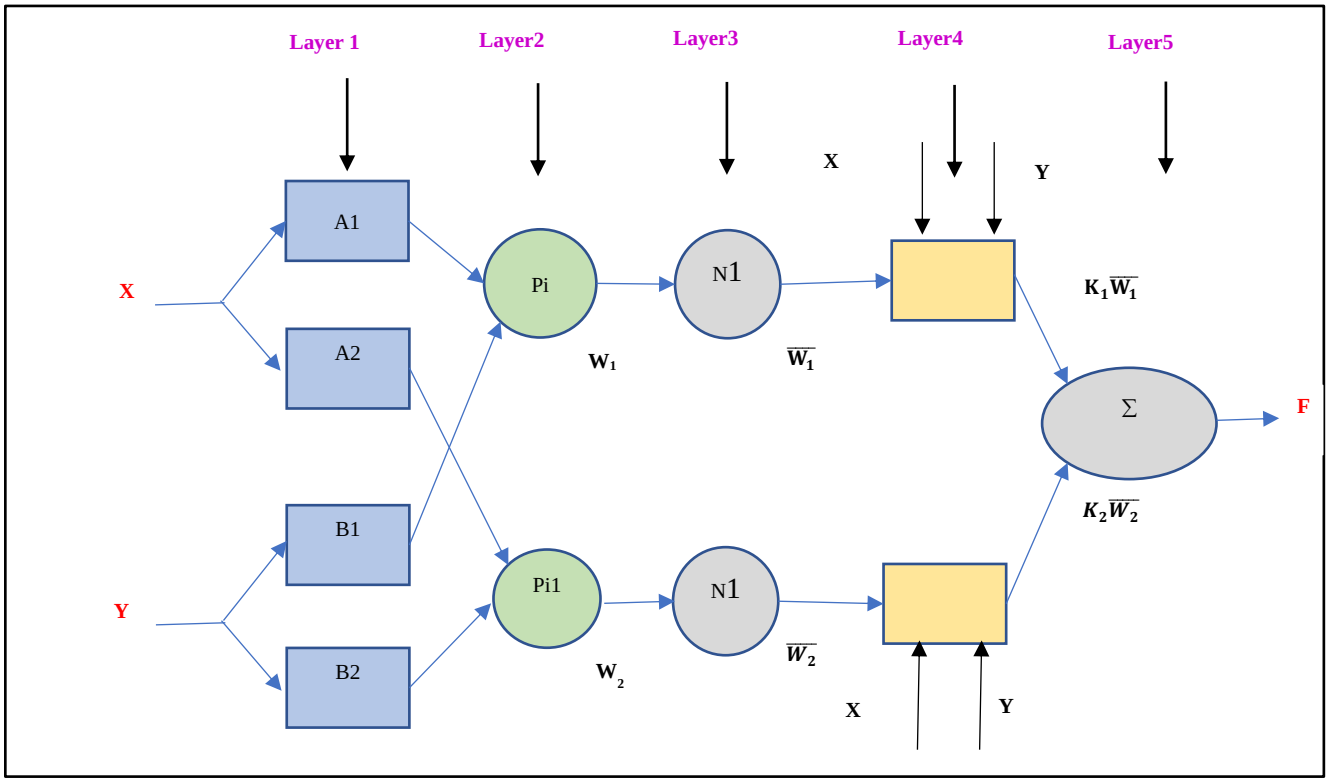

Fig. 5 Architecture of the ANFIS controller

2.3. Variable Frequency Control (VFC)

By adjusting the F_s value, the suggested converter employs VFC to control the voltage at its output. Figure 7 depicts a VFC conceptual block diagram in which a PI controller handles the error control signal (V_{error}) between the output measured voltage ($V_{measured}$) and the output required voltage ($V_{reference}$). Hence, PWM applies the control signal F_s to produce regulated switch gating pulses based on the error sign [24].

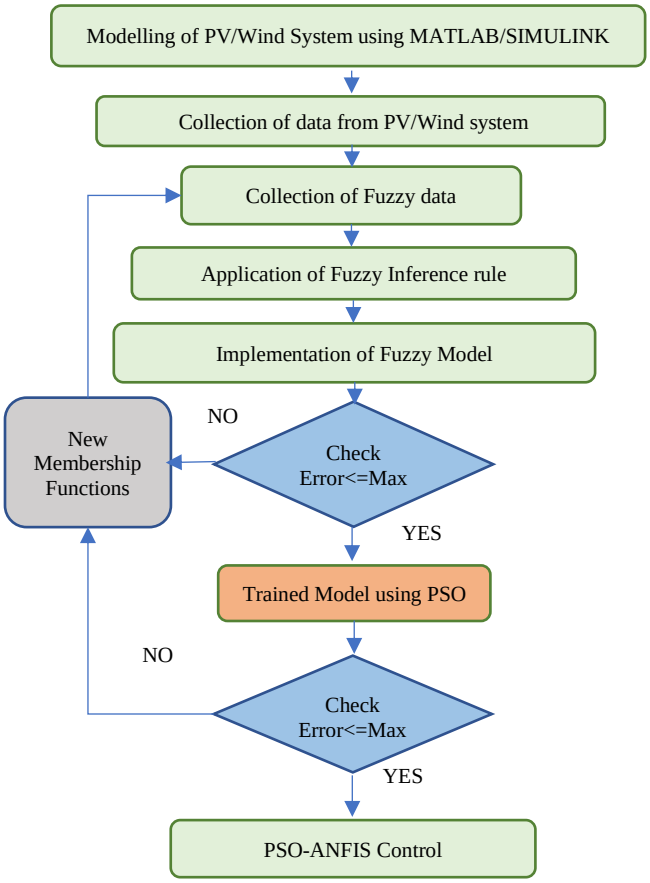

Fig. 6 An ANFIS–PSO hybrid MPPT control scheme flowchart

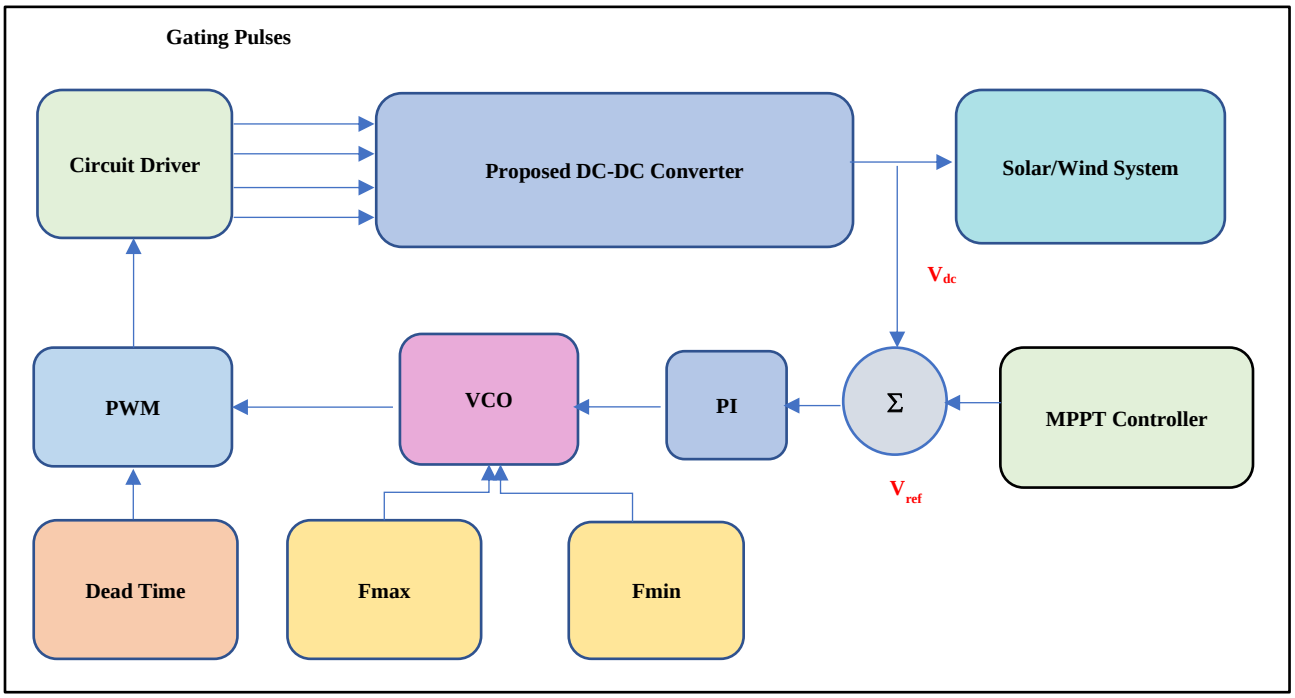

Fig. 7 The VFC's schematic representation

3. Simulation Model

The proposed HSWS simulation model, as shown in Figure 8, is simulated with Matlab/Simulink software, and the parameters used for designing are presented in Table 1. The solar array and wind system outputs are connected to dc-dc converters 1 and 2.

The control switch's duty cycle is controlled by the variable frequency controller based on the reference signal produced by the MPPT controller to change the output voltage of these two converters. A battery charging and discharging system with a bidirectional DC/DC converter keeps a consistent voltage at the DC bus.

4. Simulation Results

The preceding section's model is simulated, and the results are provided in the following section. Figure 11 shows the performance characteristics of solar system. Figure 11 shows that under STC conditions, i.e., 1000 W/m^2 solar irradiation and a 25°C panel, maximum power generation will occur, and power generation will decrease with a decrease in solar irradiation and an increase in temperature.

Table 1. Simulation model Specification

Parameters	Values	Units
Solar PV Array		
Rated power	1005	Watts
Open circuit voltage	139.6	Volts
Short circuit current	9.26	Amps
Voltage at maximum power	113.1	Volts
Current at maximum power	8.90	Amps
Standard test condition	Irradiance: 1000 W/m^2, Temp: 25 ºC	
Wind Turbine		
Rated mechanical output power	500	Watts
Rated wind speed	12	m/sec^2
Cut in wind speed	3	m/sec^2
Cut out wind speed	18	m/sec^2
DC/DC Resonant Converter 1		
Rated capacity	1000	Watts
Resonance frequency	5000	Hz
Switching frequency range	4.25-5k	Hz
Input voltage	120	Volts
Output voltage	320	Volts
Resonant inductor	150	µHenry
Resonant capacitor	60	µFarad
DC-DC Resonant Converter 2		
Rated capacity	1000	Watts
Switching frequency range	4.25-5k	Hz
Input voltage	50	Volts
Output voltage	320	Volts
Resonant inductor	200	µHenry
Resonant capacitor	70	µFarad
Battery Bank		
Number of batteries connected in series	12	units
Total battery bank voltage	144	Volts
Nominal capacity@ 20hr rate	26	Ah
Discharge current @ 20hr rate	1.3	Amps
R-Load (DC-Load)		
Total capacity	1000	Watts
The 3-Phase Interleaved Bidirectional DC-DC Converter		
Total capacity	1000	Watts
Switching frequency	10k	Hz

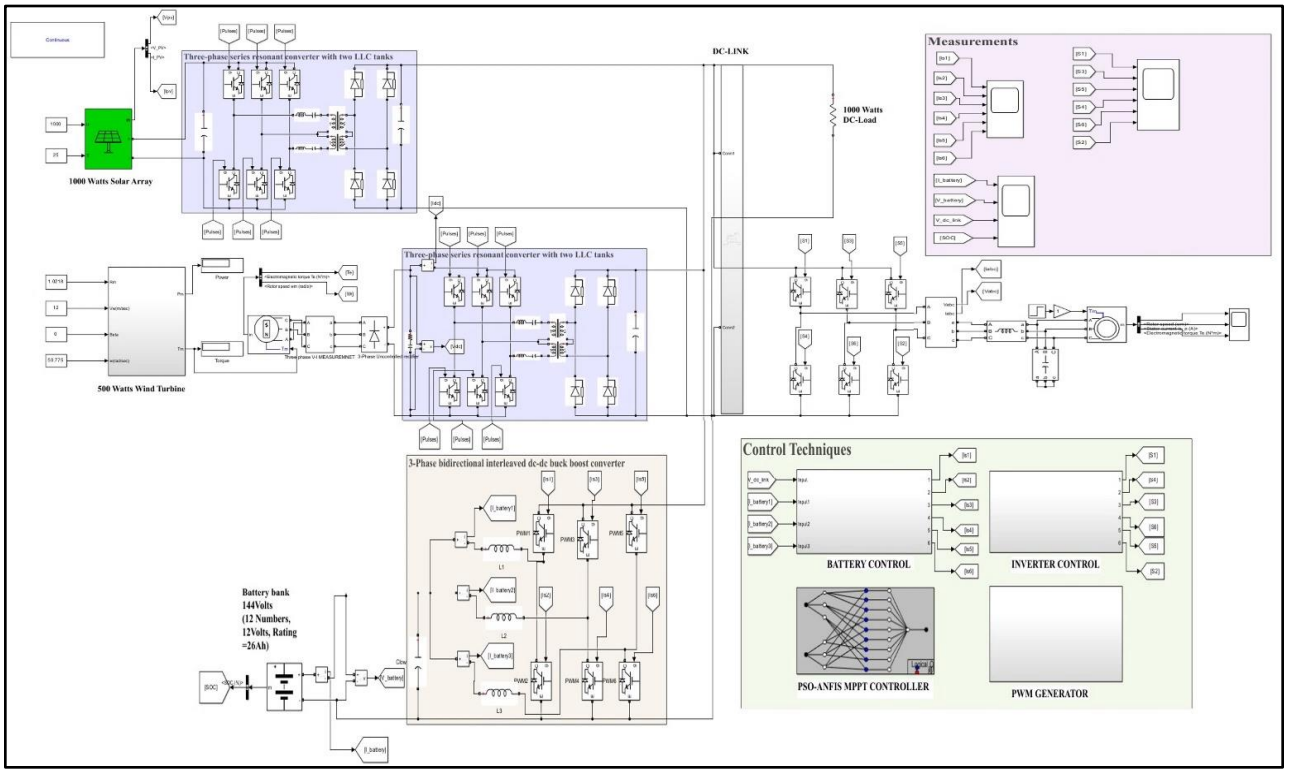

Fig. 8 Simulation model of the hybrid solar-wind system

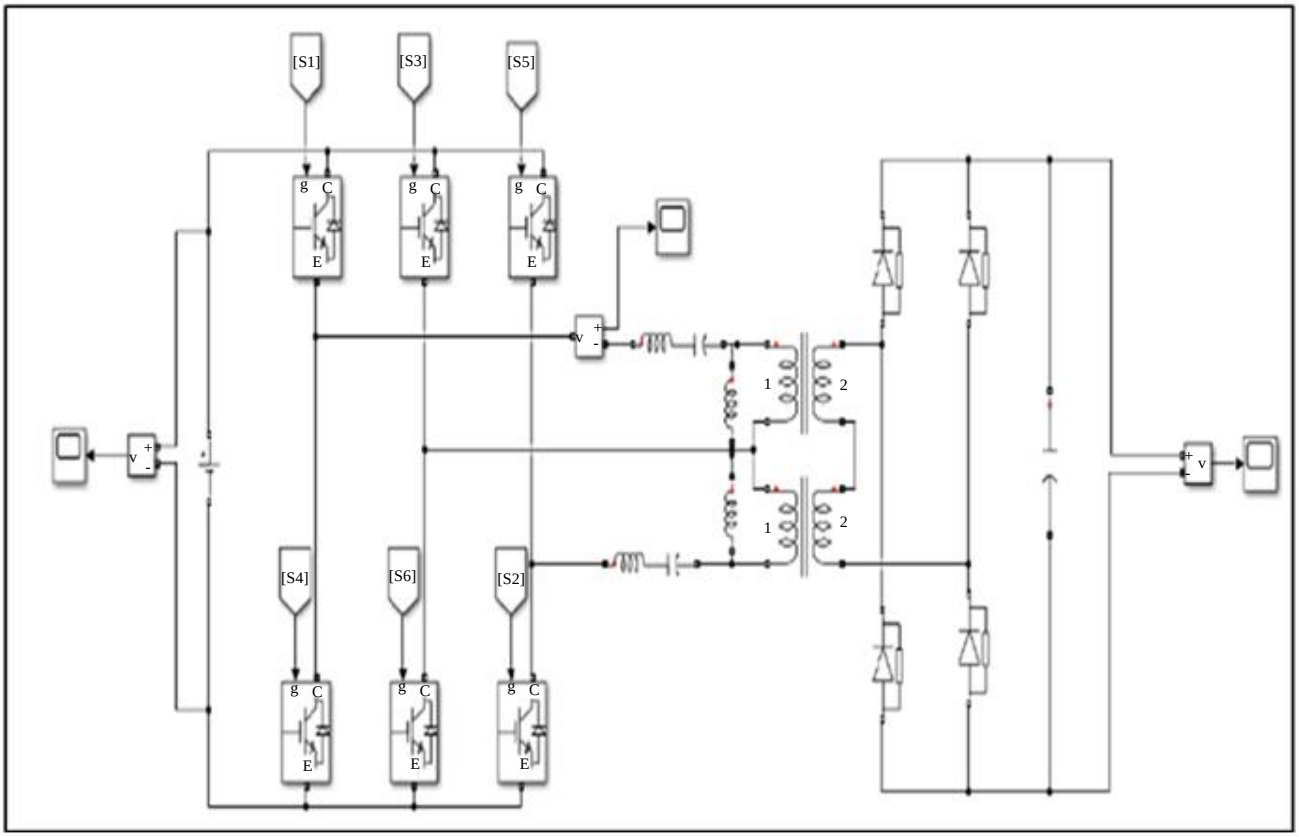

Fig. 9 Simulation model of the proposed converter

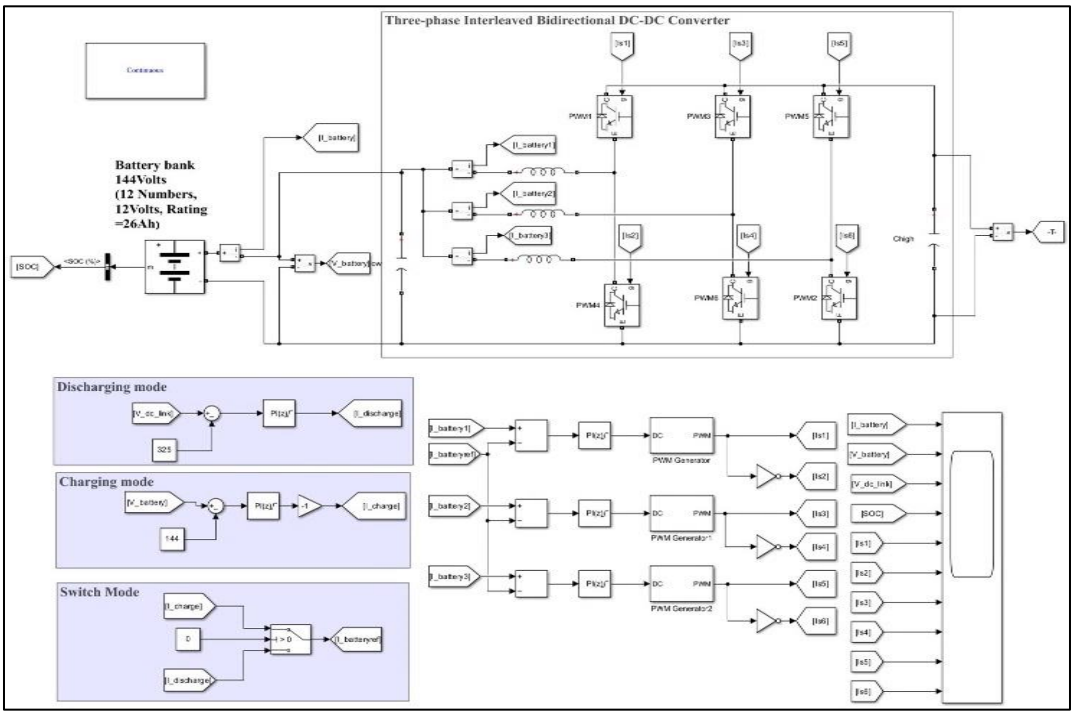

Fig. 10 Battery bank with bidirectional converter

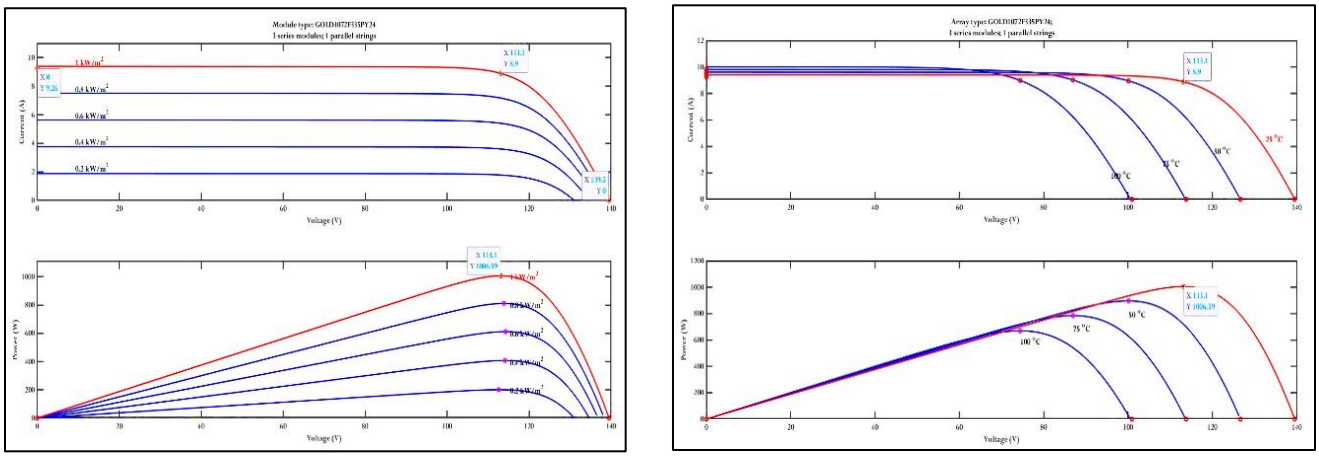

(a) **(b)**

Fig. 11 PV and VI curve of a solar array under different (a) solar irradiations (b) temperatures

Figure 12 depicts a single turbine's power vs. wind speed curve. The turbine's cut-in speed is 7 m/sec, above which the turbine generates electricity. The turbine generates rated power, i.e., 143 Watts, at rated speed, i.e., 12 m/sec. The turbine's cut-out speed is 58 m/sec, above which the turbine generates no power.

Figure 13 presents the load waveforms directly supplied by the hybrid system without a DC-DC resonant boost converter. The power supplied to the load is only 200 Watts, accounting for approximately 20% of the system's overall capacity. To match the generation with the load demand, two DC-DC converters are used, one for the solar system and one for the wind system.

Figures 14 and 15 show the simulation results of the converter coupled to a solar array, while Figures 16 and 17 show the output waveforms of a converter attached to wind turbines. The performance of both resonant converters is tested under different load situations when the load is ramped down from full load (3.11 amps) to half load (1.56 amps) at time 0.05s, as shown in Figures 20 and 21. This validates the proposed converters and their controller's ability to maintain

a consistent output voltage under dynamic load conditions. Note that 15 and 17 confirm that ZVS is possible for all switches, which is essential information. The gate and collector voltages confirm that the VCE fell to zero for each switch before the switches were turned on. For various load conditions, all switches were thus turned on at ZVS. Figure 18 demonstrates that the dc link voltage is kept constant, i.e., 320 volts, with the aid of the battery, and that the battery voltage is kept constant, i.e., 144 volts, as shown in Figure 19.

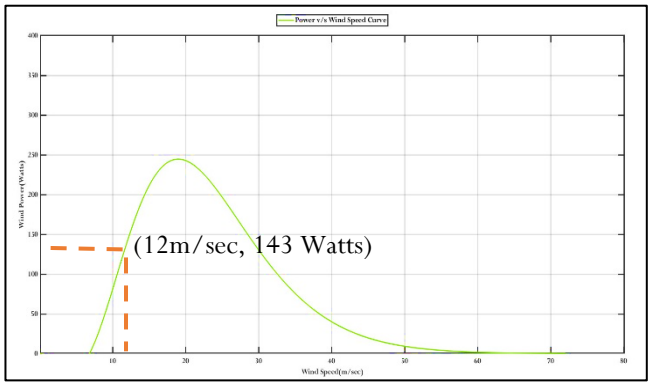

Fig. 12 Power curve for different wind speed

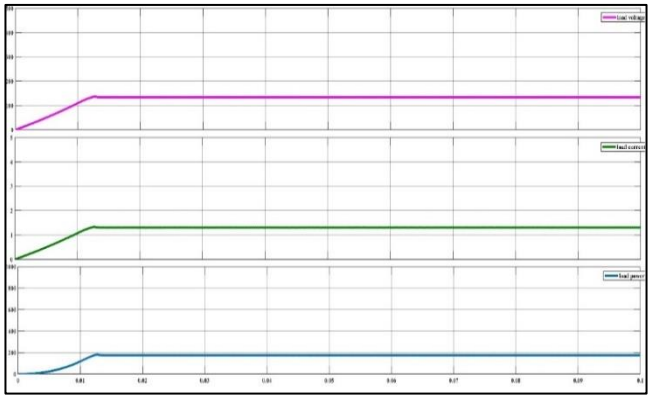

Fig. 13 Output parameters (V, I, and P) of load (without MPPT controller)

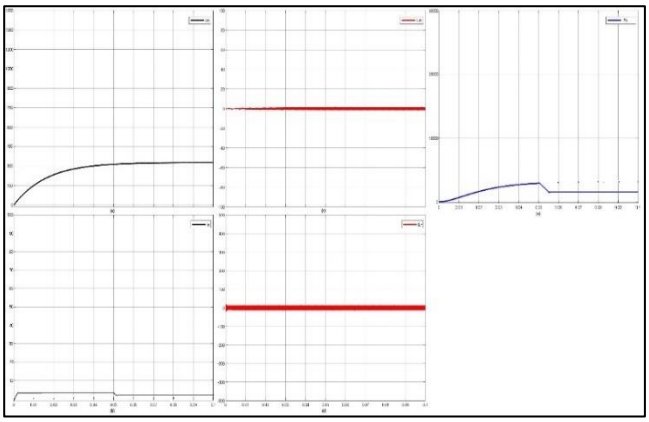

Fig. 14 Simulation waveform of the DC-DC converter1 (a) output voltage[1] (b) output current[1] (c) resonant inductor current[1] (d) magnetizing inductor current[1] (e) output power[1]

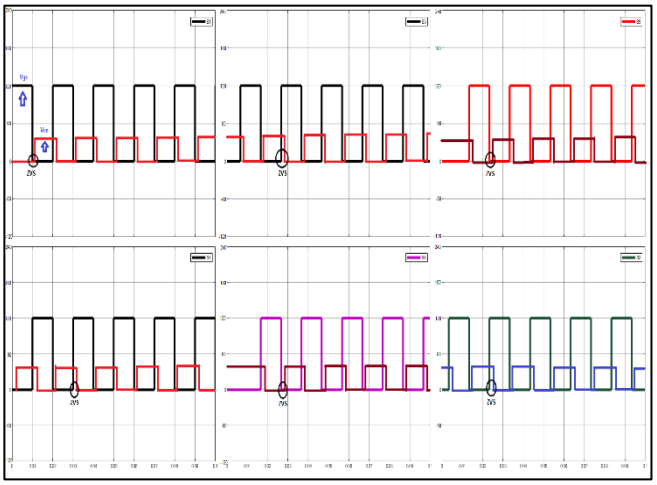

Fig. 15 Simulation output results for emitter-gate voltage (V_{GE}^1) and emitter-collector voltage (V_{CE}^1) for all switches of converter 1

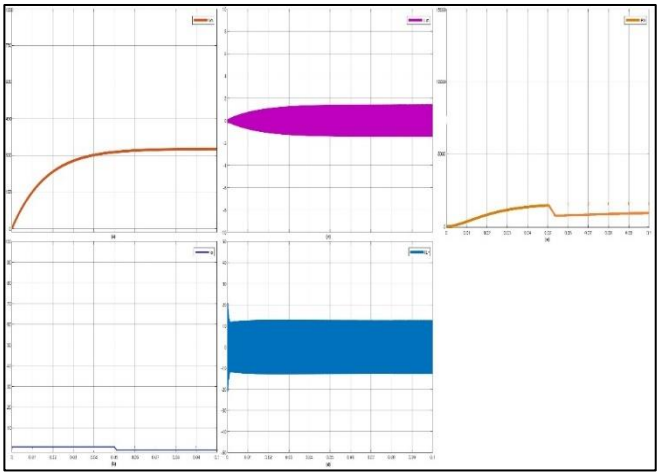

Fig. 16 Output waveform of DC-DC converter 2 (a) output voltage[2] (b) output current[2] (c) resonant inductor current[2] (d) magnetizing inductor current[2] (e) output power[2]

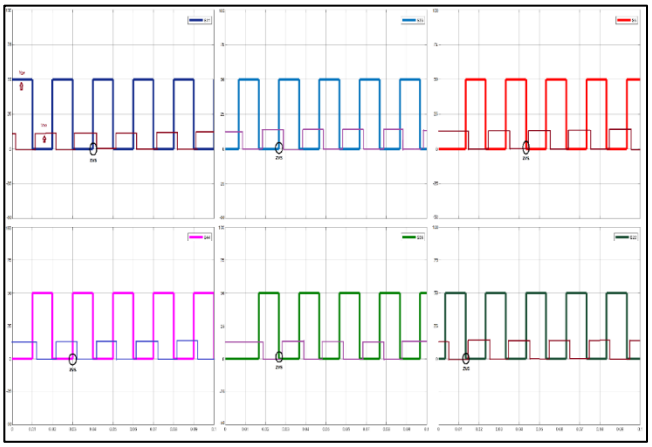

Fig. 17 Gate-emitter voltage (V_{GE}^2) and collector-emitter voltage (V_{CE}^2) of all switches of converter 2

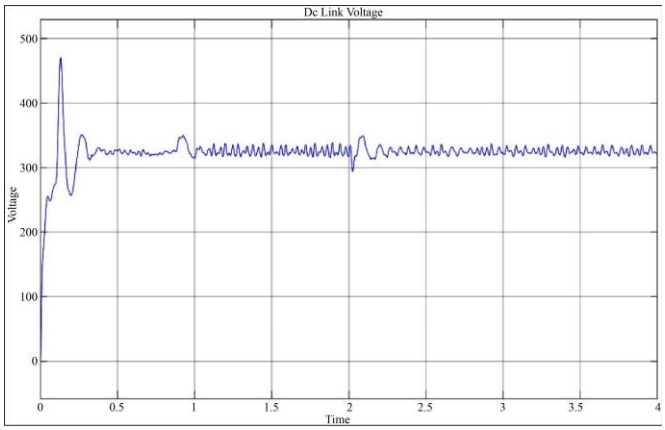

Fig. 18 DC link voltage

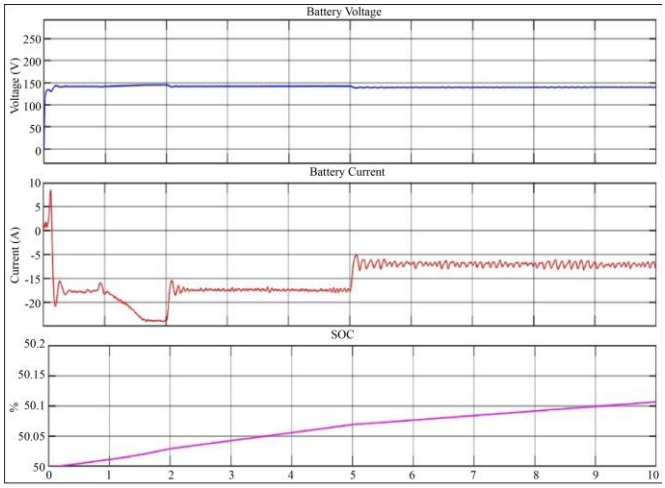

Fig. 19 Simulation outputs waveforms of a battery bank with a bidirectional converter

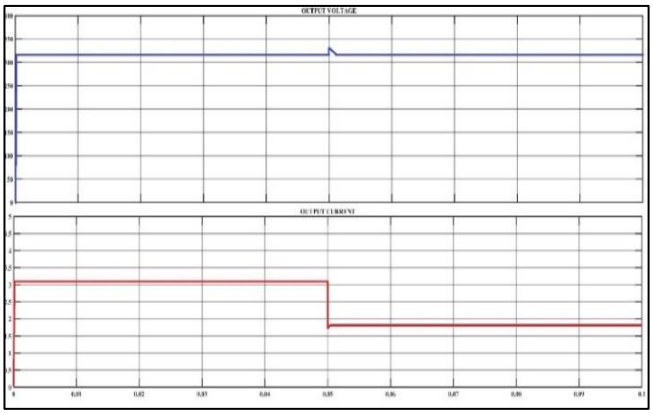

Fig. 20 Simulation response of converter 1 for load variation

5. THD Analysis

The quantity of THD produced by both DC-DC converters is determined via FFT analysis. Figure 22 displays the voltage, current, and power harmonics induced by converters 1 and 2. The THD results obtained are per the IEEE 519 standard.

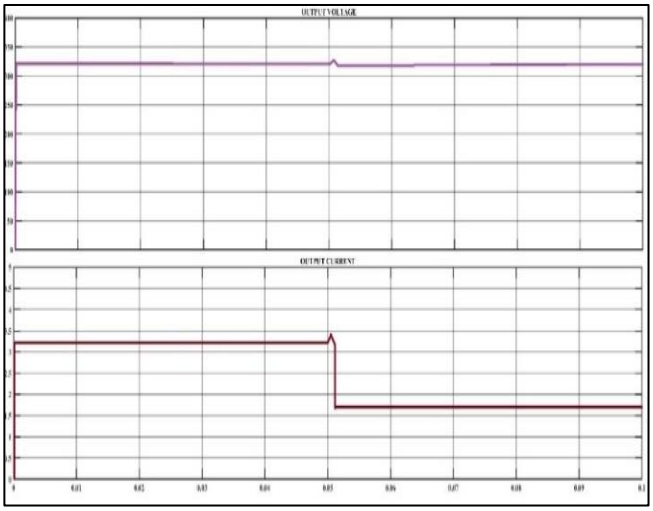

Fig. 21 Simulation result of converter 2 for load change

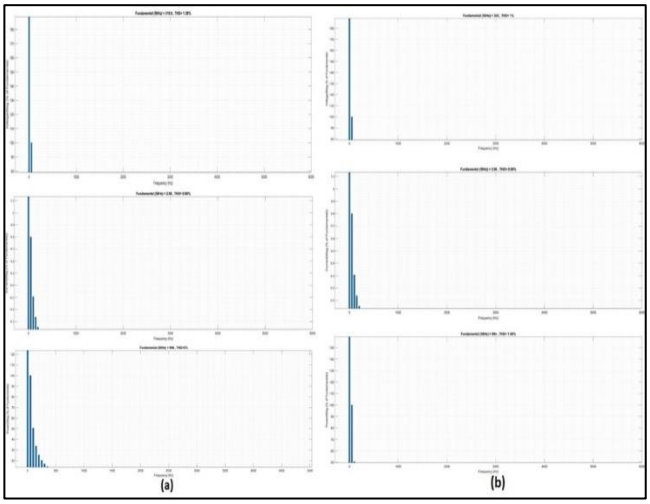

Fig. 22 THD Analysis (a) converter 1 (b) Converter 2

6. Conclusion

This research presents a three-phase resonant converter for a hybrid solar-wind system with two LLC RTs. All tanks are considered identical to assure a balanced RT variable by combining a 3-phase inverter with DLLC RTs and having both tanks share an uncontrolled full bridge rectifier. The suggested boost converter can decrease the number of switching devices, which would significantly influence the circuit's size and cost. The suggested converter's output voltage is three times greater than the input voltage for a solar array and six times for a wind system, indicating that it is suited for high-voltage applications. The proposed converters and their controllers can maintain a consistent and good output voltage quality under dynamic load conditions. For the proposed converter, VFC was used to maintain a significant load fluctuation. The ANFIS-PSO hybrid maximum power extraction approach employs a faster execution speed, high PV track efficiency, and low power loss ability, enabling rapid MPP region. A

battery bank with a bidirectional control can keep constant DC link voltage irrespective of load variation.

Further work can be done on this by using an IOT-based MPPT control approach and comparing simulation results to experimental outcomes.

References

[1] Hossein Ardi, Ali Ajami, and Mehran Sabahi, "A Novel High Step-Up DC–DC Converter with Continuous Input Current Integrating Coupled Inductor for Renewable Energy Applications," *IEEE Transactions on Industrial Electronics*, vol. 65, no. 2, pp. 1306–1315, 2017. [CrossRef] [Google Scholar] [Publisher Link]

[2] V. Vanitha, Nithya Ramesh, and R. Resmi, "Hybrid Wind and Solar Based Battery Charging Controller," *Innovations in Power and Advanced Computing Technologies (i-PACT), IEEE*, vol. 1, pp. 1–5, 2019. [CrossRef] [Google Scholar] [Publisher Link]

[3] Heena Parveen, and A. Raghu Ram, "Design and Performance Analysis of SEPIC Converter with Different MPPT Control Algorithms for Hybrid Solar-Wind System Design," *Neuro Quantology*, vol. 20, no. 19, p. 2391–2400, 2022. [CrossRef] [Publisher Link]

[4] J. Jurasz et al., "A Reviewon the Complementarity of Renewable Energy Sources: Concept, Metrics, Application and Future Research Directions," *Solar Energy*, vol. 195, pp. 703–724, 2020. [CrossRef] [Google Scholar] [Publisher Link]

[5] Mergu Chandramouly, and A. Raghuram, "Introduction to Solar Wind Hybridenergy Systems," *International Journal of Engineering Research in Electrical and Electronic Engineering*, vol. 3, 2017. [Publisher Link]

[6] Emília Inês Come Zebra et al., "A Review of Hybrid Renewable Energy Systems in Mini-Grids for Off Grid Electrification in Developing Countries," *Renewable and Sustainable Energy Reviews*, vol. 144, p. 111036, 2021. [CrossRef] [Google Scholar] [Publisher Link]

[7] Farhan Mumtaz et al., "Review on Non-Isolated DC-DC Converters and their Control Techniques for Renewable Energy Applications," *Ain Shams Engineering Journal*, vol. 12, no. 4, pp. 3747–3763, 2021. [CrossRef] [Google Scholar] [Publisher Link]

[8] Kummara Venkat Guru Raghavendra et al., "A Comprehensive Review of DC–DC Converter Topologies and Modulation Strategies with Recent Advances in Solar Photovoltaic Systems," *Electronics*, vol. 9, no. 1, p. 31, 2019. [CrossRef] [Google Scholar] [Publisher Link]

[9] Hongliang Wang et al., "A Passive Current Sharing Method with Common Inductor Multiphase LLC Resonant Converter," *IEEE Transactions on Power Electronics*, vol. 32, no. 9, pp. 6994–7010, 2016. [CrossRef] [Google Scholar] [Publisher Link]

[10] Mohamed Salem et al., "Improved Topology of Three-Phase Series Resonant DC-DC Boost Converter with Variable Frequency Control," *Alexandria Engineering Journal*, vol. 61, no. 2, pp. 1701–1713, 2022. [CrossRef] [Google Scholar] [Publisher Link]

[11] Maria Teresa Outeiro, Giuseppe Buja, and Dariusz Czarkowski, "Resonant Power Converters: An Overview with Multiple Elements in the Resonant Tank Network," *IEEE Industrial Electronics Magazine*, vol. 10, no. 2, pp. 21–45, 2016. [CrossRef] [Google Scholar] [Publisher Link]

[12] Mohamed Salem et al., "Comparison of LCL Resonant Converter with Fixed Frequency, and Variable Frequency Controllers," *IEEE Conference on Energy Conversion, IEEE*, pp. 84–89, 2017. [CrossRef] [Google Scholar] [Publisher Link]

[13] Michael W. Condry, "The IEEE Industrial Electronics Society and the Technology Management Council [My View]," *IEEE Industrial Electronics Magazine*, vol. 4, no. 2, pp. 56–56, 2010. [CrossRef] [Google Scholar] [Publisher Link]

[14] Ahmed S. Ragab, Naggar H. Saad, and Ahmed A. El-Sattar, "LLC Resonant DC-DC Converter for Grid-Connected PV System," *12th International Conference on Computer Engineering and Systems, IEEE*, pp. 279–285, 2017. [CrossRef] [Publisher Link]

[15] Mohamed Salem et al., "Resonant Power Converters with Respect to Passive Storage (LC) Elements and Control Techniques– An Overview," *Renewable and Sustainable Energy Reviews*, vol. 91, pp. 504–520, 2018. [CrossRef] [Google Scholar] [Publisher Link]

[16] Olalekan Kunle Ajiboye et al., "Hybrid Renewable Energy System Optimization via Slime Mould Algorithm," *International Journal of Engineering Trends and Technology*, vol. 71, no. 6, pp. 83-95, 2023. [CrossRef] [Google Scholar] [Publisher Link]

[17] Mergu Chandramouly, and A. Raghuram, "Performance of Hybrid Solar-Wind Energy Generating System - Prototype Model," *YMER*, vol. 21, p. 1779, 2022. [Publisher Link]

[18] Sourabh Goyal et al., "Solar-Wind Hybrid Systems for Power Generation," *SSRG International Journal of Mechanical Engineering*, vol. 6, no. 5, pp. 14-21, 2019. [CrossRef] [Publisher Link]

[19] Mohamed Salem et al., "Three-Phase Series Resonant DC-DC boost Converter with Double LLC Resonant Tanks and Variable Frequency Control," *IEEE Access*, vol. 8, pp. 22386–22399, 2020. [CrossRef] [Google Scholar] [Publisher Link]

[20] Neeraj Priyadarshi et al., "An Extensive Practical Investigation of FPSO-Based MPPT for Grid Integrated PV System under Variable Operating Conditions with Anti-Islanding Protection," *IEEE Systems Journal*, vol. 13, no. 2, pp. 1861–1871, 2018. [CrossRef] [Google Scholar] [Publisher Link]

[21] Neeraj Priyadarshi et al., "An Experimental Estimation of Hybrid ANFIS–PSO-Based MPPT for PV Grid Integration under Fluctuating Sun Irradiance," *IEEE Systems Journal*, vol. 14, no. 1, pp. 1218–1229, 2020. [CrossRef] [Google Scholar] [Publisher Link]

[22] V. Seydi Ghomsheh, M. Aliyari Shoorehdeli, and M. Teshnehlab, "Training ANFIS Structure with Modified PSO Algorithm," *Mediterranean Conference on Control & Automation, IEEE*, pp. 1–6, 2007. [CrossRef] [Google Scholar] [Publisher Link]

[23] Nidhi Haryani, Rolando Burgos, and Dushan Boroyevich, “Variable Frequency and Constant Frequency Modulation Techniques for GaN based MHz H-bridge PFC,” *IEEE Applied Power Electronics Conference and Exposition, IEEE*, pp. 1889–1896, 2015. [CrossRef] [Google Scholar] [Publisher Link]

[24] S. Priyanka et al., "IOT based Hybrid Artificial Tree for Solar/Wind Power Generation with Pollution Control and Monitoring," *SSRG International Journal of Computer Science and Engineering*, vol. 8, no. 4, pp. 1-3, 2021. [CrossRef] [Google Scholar] [Publisher Link]